Journal Pre-proof

Electrodynamic single-particle trap integrated into double-cavity ring-down spectroscopy for light extinction

A. Valenzuela, E. Bazo, R.A. Rica, L. Alados-Arboledas, F.J. Olmo-Reyes

Please cite this article as: Valenzuela A, Bazo E, Rica RA, Alados-Arboledas L, Olmo-Reyes FJ, Electrodynamic single-particle trap integrated into double-cavity ring-down spectroscopy for light extinction, *Journal of Aerosol Science* (2023), doi: https://doi.org/10.1016/j.jaerosci.2023.106292.

This is a PDF file of an article that has undergone enhancements after acceptance, such as the addition of a cover page and metadata, and formatting for readability, but it is not yet the definitive version of record. This version will undergo additional copyediting, typesetting and review before it is published in its final form, but we are providing this version to give early visibility of the article. Please note that, during the production process, errors may be discovered which could affect the content, and all legal disclaimers that apply to the journal pertain.

Electrodynamic single-particle trap integrated into double-cavity ring-down spectroscopy for light extinction

A. Valenzuela[+,‡,*], E. Bazo[+,‡], R.A. Rica[‡,#], L. Alados-Arboledas[+,‡] and F.J. Olmo-Reyes[+,‡]

[+]Andalusian Institute for Earth System Research (IISTA-CEAMA), Granada 18006, Spain

[‡]Universidad de Granada, Department of Applied Physics, Granada 18071, Spain

[#]Research unit Modelling Nature (MNat), Granada 18071, Spain

ABSTRACT:

The study of the interaction of light with matter upon changing environmental conditions requires new platforms that provide accurate and reliable measurements. One suitable technique for studying such interaction uses electrodynamic traps to levitate micro or nanoparticles in combination with an optical interrogation technique, but improvements and new developments that complement spectroscopic information are necessary. Here, we use a Paul Electrodynamic Trap (PET) coupled to a Double-Cavity Ring Down Spectroscopy (D-CRDS) to measure the extinction cross section of single levitated particles at two different wavelengths (405 and 532 nm). The level of control achieved over the motion and stability is such that the particle can be consecutively placed at the central maximum of two independent TEM_{00} Gaussian modes of the ring-down cavities. Therefore, we can directly measure the dynamic change of the extinction cross section of a single particle at two different wavelengths. The combination of simulations using Mie theory and experiments demonstrates the potential of this robust and versatile setup applied to 1,2,6-hexanetriol particles. Unlike standard methods, our system provides crucial information of drastic and reversible change in the extinction cross-section of a sodium chloride particle in efflorescence and deliquescence points, indicating changes in solute mass, charge, refractive index, sphericity and size during the dehydration and hydration processes.

KEYWORDS: single levitated particle, electrodynamic trap, cavity ring down spectroscopy, extinction cross section, elastic scattering, climate change.
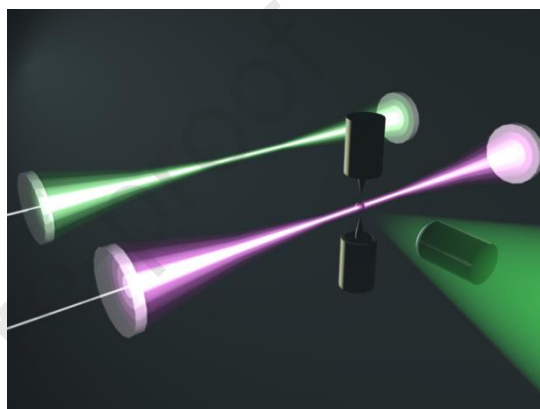
1. INTRODUCTION

Manipulating individual particles offers the only opportunity to accurately probe the intrinsic physicochemical properties at a fundamental level without the complexity associated with the ensemble of particles. Single particle characterization needs two basic requirements, namely, to capture, confine and precisely control a single specimen of interest, and a highly sensitive, non-invasive optical interrogation technique.

Trapping based on optical forces like conventional optical tweezers is one of the most common techniques that facilitate the confinement and tracking of a single particle, relying mainly on two forces: the scattering and the gradient forces (Bain and Preston, 2019). Its use for the evaluation of microparticles and nanoparticles has been pioneered in numerous studies related to fundamental research in aerosol science and hygroscopic behavior (Davies, 2019; Gregson et al., 2018; Hart et al., 2015; Krieger and Braun, 2001; Mason et al., 2015; Walker et al., 2013; Zardini et al., 2006). Nevertheless, these types of traps are limited to weakly absorbing materials (Bain et al., 2018). If a strongly absorbing particle is illuminated from one side, then gas molecules on the higher temperature side of the particle will have higher velocities due to collisions with the hot side of the particle, imposing a net force (photophoretic force) pushing the particle towards its cold side. For a strongly absorbing particle, this photophoretic force can be 4 to 5 orders of magnitude stronger than the gradient force, pushing the particle out of the capture zone. Recently, several methods have been proposed to enable optical trapping of absorbing airborne particles using the photophoretic force (Gong et al., 2017). The main drawback stems from the fact that the high power required for trapping causes heating which will lead to photodeterioration and a change in the physicochemical composition when the particles contain volatile species. From the geometric point of view, the poor stability of irregular particles in optical traps is due to the imbalance of forces coming from the different faces that have different scattering forces associated with them (Gong et al., 2018). An attractive alternative to optical trapping is the use of electric fields to capture charged particles. The electrodynamic trapping device, also called Paul trap, offers advantages because it can levitate any charged object regardless of its optical properties. The electrodynamic Paul trap (PET) uses a combination of AC and DC electric fields for the confinement of charged particles (Archer et al., 2020; Krieger and Braun, 2001; Lin et al., 2015; Mason et al., 2015; Walker et al., 2013; Zardini et al., 2006).

The measurement of the phase function of elastically scattered light is a consolidated approach to obtain information about size distributions, morphologies, and the real part of the complex refractive index (m_λ), n_λ, of aerosol particles, (David et al., 2016; L. Price et al., 2020) n_λ describing the phase velocity of light inside particles. The typical interference pattern obtained between light passing through a particle and that passing close to the edge can be measured and compared with Lorenz-Mie theory to estimate particle size (Cotterell et al., 2017; Valenzuela et al., 2020). However, gaining exploitable information when the particle absorbs light, or it is not a perfect sphere is a major challenge because the phase function loses contrast. Under these conditions, independent measurements of how the particle extinguishes radiation could shed light on previously unreported details of the particle's response to changes in the conditions to which it is exposed.

The flux of light scattered and absorbed by a single homogeneous spherical particle is determined by the extinction cross-section, $\sigma_{ext,\lambda}$. A window of possibilities is opened by probing the variation of $\sigma_{ext,\lambda}$ of single particles that absorb light, have irregular geometry, or are exposed to changing environmental conditions. The spectroscopic analysis is an exciting route towards these ends, and among them, cavity ringdown spectroscopy (CRDS) is particularly fine-tuned, as well as an excellent identifier of the physicochemical particle footprint. This approach has been initially applied in the analysis of aerosols to measure the light extinction caused by an ensemble of particles leading to an unpreventable loss of single-particle information (Dinar et al., 2008; Hasenkopf et al., 2010; Mason et al., 2012; Miles et al., 2011; Pettersson et al., 2004). Further, an improvement in the accuracy of obtaining reliable $\sigma_{ext,\lambda}$ values has been achieved through CRDS measurements of a single trapped initially non-absorbing particle in combination with independent estimation of particle size, allowing an alternative assessment of the n_{λ} (Mason et al., 2012; Walker et al., 2013). Recent advances in the trapping field have demonstrated the possibility of characterizing light-absorbing and irregularly shaped specimens by integrating a focused hollow beam trap into a cavity ring down spectroscopy system (Gong et al., 2017). Nevertheless, only qualitative quantities were presented. Less is known about the effect on light extinction due to the irregular geometrical shape of the particle. In this regard, Valenzuela et al. (2021) integrated a linear electrodynamic quadrupole into a CRDS by evaluating continuous $\sigma_{ext,405}$ measurements after a single inorganic particle experimented efflorescence. Fitting the $\sigma_{ext,405}$ values to a superellipsoid model allowed estimation of the aspect ratio of the crystallized particle. Using the latter configuration, Knight et al. have already successfully measured the absorption through the evolution of the imaginary refractive index, k_{λ}, for two-component particles composed of nigrosine and 1,2,6-hexanetriol (Knight et al., 2022). Therefore, a combination of electrodynamic traps and CRDS is a convenient tool to work with, since it can provide valuable information not accessible to optical trapping approaches, as many particles in the atmosphere absorb light or have an irregular shapes.

An open question hardly addressed is the spectral dependence of the dynamic change of $\sigma_{ext,\lambda}$ for one single trapped particle. Gathering more independent spectroscopic data in the same experiment may reduce the space over which parametrize optical properties. As an example, spectral aerosol optical depth (δ_{λ}) is generally the key parameter to study atmospheric aerosols and their optical indices (Cachorro et al., 2001). The wavelength dependence of the δ_{λ} varies because of the aerosols type and their physical and chemical characteristics. This wavelength dependence is expressed by the Angstrom exponent (α). The derivation of α can be a useful tool to distinguish and characterize the different aerosol types in relation to its size (Schuster et al., 2006):

$$\delta_{\lambda} = \beta \lambda^{-\alpha} \qquad (1)$$

where, λ is the wavelength, β is the aerosol optical depth at 1 µm wavelength. α can be computed from spectral values of δ_{λ} by rationing Eq. (1) at two different wavelengths, λ_1 and λ_2, through the expression:

$$\alpha = -\frac{d\ln\delta}{d\ln\lambda} = -\frac{\ln\left(\frac{\delta_{\lambda 2}}{\delta_{\lambda 1}}\right)}{\ln\left(\frac{\lambda_2}{\lambda_1}\right)} \qquad (2)$$

From this expression α is the negative of the slope, or the negative of the first derivative of δ_λ versus wavelength in logarithmic scale. As particles increase in size, the value of α decreases. Typical values of α range from > 2.0 for fresh smoke particles to nearly zero for Sahelian/Saharan desert dust cases (Valenzuela et al., 2015):

The δ_λ for the atmospheric column depend on the $\sigma_{ext,\lambda}$ values. For our laboratory measurements with individual particles, the equivalent Angstrom law can be expressed as:

$$\sigma_{ext,\lambda} = \beta\lambda^{-\alpha} \qquad (3)$$

Having $\sigma_{ext,\lambda}$ at another wavelength for the same aerosol allows to accurately determine α. Determining α with this experimental setup for many particle sizes and considering the influence of relative humidity on particle size growth will provide with a more precise relationship between mean particle size and α value.

Looking for new configurations to improve the optical and microphysical information obtained from aerosols, we present in this work a new setup combining a Paul Electrodynamic Trap (PET) and a Double-Cavity Ring Down Spectroscopy (D-CRDS) system (see Figure 1). The novelty of this single particle cavity ring down setup with respect to previous CRDS configurations is the possibility to move the PET on a rail transverse to the two parallel cavities with the initial particle held stationary levitating in the trap (see Figure 1b). The new configuration allows to retrieve, for the first time, the elastic scattering at 473 and 532 nm wavelengths and $\sigma_{ext,\lambda}$ for the 532-CRDS and 405-CRDS systems from the very same trapped particle. This new capability will remove uncertainties due to the natural variability between different particles, leading to improved measurements. The spectral selective setup is a versatile working platform, adding enormous flexibility by optically interrogating the same trapped particle at two different wavelengths with excellent stability and reproducibility. The robust PET facilitates manipulations and control of the trapped particle with high sensitivity, holding the particle right at the central maximum of two independent TEM$_{00}$ Gaussian modes of the ring-down cavities, obtaining highly resolutive dynamic change of ring down time data. We validate the system with 1,2,6-hexanetriol (HT) and sodium chloride particles and compare Lorenz-Mie theory with experimental data in terms of $\sigma_{ext,\lambda}$ values. Further, the new system provides exploitable ring down time data for non-spherical solid particles.

2. EXPERIMENTAL SETUP AND METHODOLOGY

A schematic diagram of the combined PET and D-CRDS platform and an artistic representation of the trapping scheme are shown in Figs. 1. The PET is located inside a custom-made chamber and operated at atmospheric pressure and room temperature, with all measurements performed around 295 K. This platform is formed by two conical electrodes separated by 1.5 mm that are enclosed by grounded cylindrical shields which have a diameter of 2 cm and 3 cm of length. An AC voltage signal is applied to the cones; the typical operation amplitude range of the AC field is between 1 kV$_{pp}$ and 2 kV$_{pp}$ at a frequency ranging from 1 kHz to 2 kHz. By establishing the above values, the PET is capable of trapping particles ranging between 700 nm up to a few micrometers in radius.

1   The RH inside the trapping cell is monitored using a capacitance probe (Honeywell). The
2   RH is controlled by passing dry nitrogen through two MKS mass flow controllers, one
3   for dry N_2 and the other for wet N_2 and varying the ratio between the two. The mixture of
4   both flows is introduced from the top of the chamber at flow rates up to 20 cm^3/min. The
5   aerodynamic force on the particle is small, so it does not significantly affect its position.

6
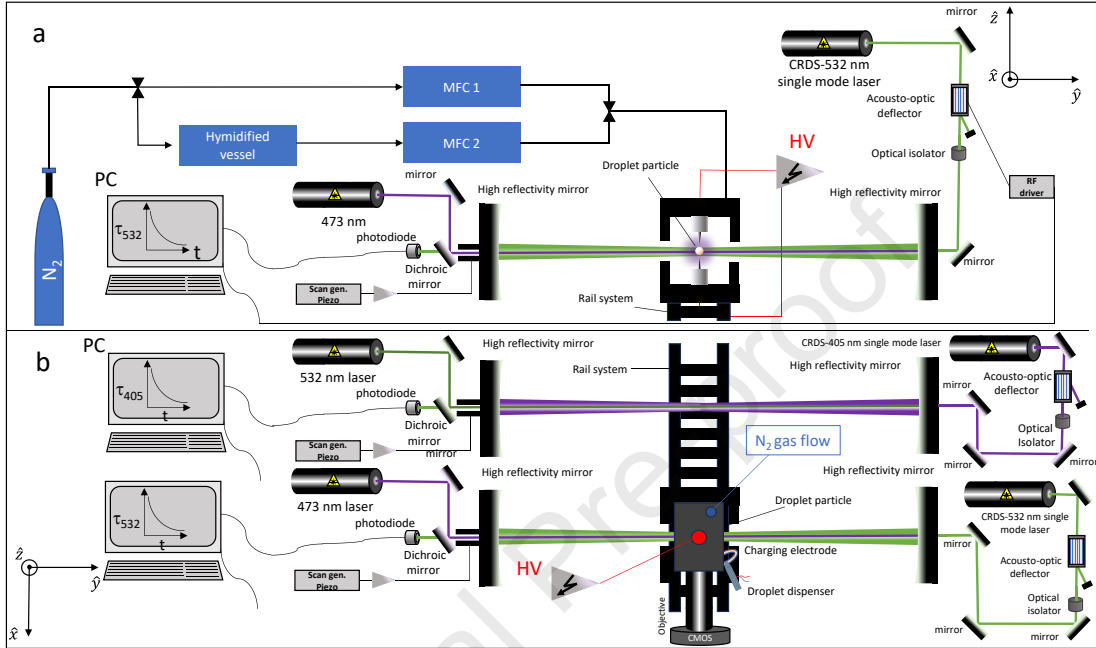
7   **Figure 1**. a) Scheme of the double cavity ring down spectroscopy setup, relativity humidity control
8   system and the Paul Electrodynamic Trap (PET) seen from the front and b) seen from the top.

9

10 Here, we use two independent and parallel CRDS (axial axis 10 cm apart), at 405 and 532
11 nm wavelengths, to measure $\sigma_{ext,\lambda}$ of the same single confined and levitated particle
12 placed right at the central maximum of TEM$_{00}$ Gaussian mode of the cavity beam by
13 carefully positioning the PET with micro. The PET is robustly fitted to a rail on which it
14 can move transversely to the axial axes of the cavities even with a trapped particle. The
15 laser beams are gently focused through an acousto-optical deflector (AOD) for each
16 wavelength that deflects the incoming beam into the cavity, and only when it is switched
17 off does the light no longer reach the cavity, triggering a ringdown event. The 1 m long
18 optical cavity for each CRDS is formed by two highly reflective mirrors (> 99.987% and
19 99.985% reflectivities at 532 and 405 nm, respectively) with a radius of curvature of 1 m.
20 In each CRDS one of the mirrors is mounted on a piezo ring actuator (Piezomechanik),
21 which translates the mirror along the axis of the cavity, periodically sweeping the cavity
22 into resonance with the laser and allowing build-up on a single longitudinal mode. The
23 piezo ring actuator is driven with a triangular waveform of amplitude 10 V at a fixed
24 frequency in the range 2-10 Hz. The estimated beam waist ($w_{0,\lambda}$) at the focal point and
25 the ring down time for the empty cavity ($\tau_{0,\lambda}$) are ~291 µm and 21.00 ± 0.19 µs,
26 respectively, for 532-CRDS system, being ~273 µm and 14.50 ± 0.23 µs, respectively,
27 for 405 CRDS system. To reduce the contributions of airborne dust particles to light
28 extinction and to prevent the mirrors getting dirty, nitrogen gas flows are directed across

5

the faces of the cavity mirrors through flow tubes that extend to a trapping cell at the center of the cavity. Measurements are made of the time constants for exponential decay of light from the TEM$_{00}$ mode when the cavity is empty ($\tau_{0,\lambda}$) and when it contains particle (τ_λ). The difference in the reciprocals of these ring-down times is proportional to the $\sigma_{ext,\lambda}$ given for the following equation:

$$\sigma_{ext,\lambda} = \frac{\pi w_{0,\lambda}^2 L}{2c}\left(\frac{1}{\tau_\lambda} - \frac{1}{\tau_{0,\lambda}}\right) \tag{4}$$

where $w_{0,\lambda}$ is the theoretical beam waist in the geometer center of cavity, L is the length of the cavity and c is the speed of light.

The light trapped within an optical cavity forms a standing wave along the cavity axis $\hat{y}$, which arises from the interference of two counter-propagating plane waves. Miller and Orr-Ewing (2007) defined an equation that modifies the Mie extinction cross-section to correctly account for the effect of the standing wave structure on measurements in a ring-down cavity. Mie $\sigma_{ext,\lambda}$ values depending on the position of particle in the standing wave with limits established in anti-node ($ky_0 = 0$) and node ($ky_0 = \frac{\pi}{2}$) positions. Particle centered half-way between a node and an anti-node ($ky_0 = \frac{\pi}{4}$) agrees exactly with the Mie theory prediction of $\sigma_{ext,\lambda}$. The equivalence of the Cavity Standing Wave Generalized Lorenz-Mie theory (CSW-GLMT) predicted CRDS measurements of $\sigma_{ext,\lambda}$ for the case $ky_0 = \frac{\pi}{4}$ and the Mie theory predicted $\sigma_{ext,\lambda}$ for a traveling wave have been exploited by Cotterell et al. (2022). Therefore, although the sampling rate in our experiment is greater than 5 Hz, since the timescales for changes in optical properties such as size and n_λ are larger than 1 second, we average our measurements at 1 Hz intervals. That way our $\sigma_{ext,\lambda,1Hz}$ values converge to the Mie theory limit.

The variation in r and n_λ is determined by fitting the complete measured $\sigma_{ext,\lambda,1Hz}$ data set to theoretical $\sigma_{ext,\lambda,Mie}$ calculated using the Mie theory in a self-consistent step. Therefore, we parameterise n_λ in terms of particle radius using the expression:

$$n_\lambda = n_{0,\lambda} + \frac{n_1}{r^3} + \frac{n_2}{r^6} \tag{5}$$

in which r is the particle radius, n_1 and n_2 are fitting parameters, and $n_{0,\lambda}$ is the real refractive index either of the particle in the limit of infinite size (pure HT) or is the real refractive index of pure water (1.338) (Cotterell et al., 2022).

The best fit is calculated using the reduced cumulative fractional difference (CFD$_R$):

$$CFD_R = \frac{1}{N}\sum_{i=1}^{N}\frac{\left|\sigma_{ext,\lambda,Mie} - \sigma_{ext,\lambda,1Hz}\right|}{\sigma_{ext,\lambda,1Hz}} \tag{6}$$

where $\sigma_{ext,\lambda,Mie}$ is the theoretical extinction cross section and N is the number of different particle radius used. The CFD$_R$ is calculated for a wide range of n_λ and r values, and the value of n_λ and r that gives the lowest CFD$_R$ are taken to be these either for HT or for aqueous sodium chloride particle according with the experiment.

A CMOS camera (Thorlabs, DCC1546M) coupled to a 20× long working distance lens (Mitutoyo) with a numerical aperture (NA) of 0.42, oriented at 90° to the D-CRDS laser

beam, is used to collect scattering light from a single trapped particle. This two-dimensional (2D) image is often referred to as a phase function and is transformed into one-dimensional (1D) spectra by averaging each column of the image. The resulting 1D spectrum is then compared to a library of spectra calculated with Mie theory for a physically plausible range of radii and refractive indices. Correlation analysis is used to compare the calculated and experimental spectra to determine the best fit. While operating the 532-CRDS system, a horizontally propagating 473 nm Gaussian laser beam illuminates the particle for elastic scattering measurements. Keeping the same particle trapped, we move the PET on the rail to the 405-CRDS system. In this configuration, an additional horizontally propagating Gaussian laser beam at 532 nm illuminates the same particle. The dispersion on n_λ from elastic scattering can be estimated by having this optical property at different wavelengths according with the procedure detailed by Valenzuela et al.[24] Camera images indicated that the maximum horizontal particle displacement during an entire set of measurements is ∼15 μm.

3. RESULTS AND DISCUSSION
3.1. Sensitivity of the instrument

To test the potential of our system, we evaluate the sensitivity, stability, and replicability of the phase functions and the $\sigma_{ext,\lambda}$ measurements with particles whose physico-chemical properties are well characterized (1,2,6-hexanetriol, HT, and sodium chloride, NaCl). $\tau_{0,532}$ of the empty cavity is 21.00 ± 0.19 μs for the 532-CRDS system where we consider the error as 1-standard deviation after 3-minutes measurements. The error comes from the inherent noise by losses in the high reflection mirrors, scattering with dust in suspension and from molecular scattering. Taking this error into account, the minimum particle radius that the system can detect is 171 nm. However, it will also depend on the minimum particle size that the trapping system is able to confine. It has been recently shown that Paul traps can be efficiently coupled with optical cavities or other robust optical detection schemes to levitate particles well into the accumulation mode (diameter 0.1-2 μm) which is of relevant interest in the field of atmospheric climate (Bykov et al., 2019; Conangla et al., 2020, 2018; Millen et al., 2020). In the case of the 405-CRDS system the value of the $\tau_{0,405}$ without particle is 14.50 ± 0.23 μs. The inclusion of the ultraviolet wavelengths is not only crucial for the sizing of accumulation mode particles, but it also allows the retrieval of refractive indices in a range where such data are scarce but desperately needed. The D-CRDS system is sufficiently sensitive to differentiate the extinguished energy according to the part of the standing wave with which the particle interacts. However, due to the Brownian motion that the particle can experience in the three directions of space (x,y,z), the noise of the system, and the excursions that the particle undergoes when its size is resonant with the wavelength, the curve of τ_λ values show considerable width. In addition, the typical diameter of the particles we work with can be several orders of magnitude larger than the wavelength, so the value will have an associated uncertainty. Once the particle is trapped, by micrometric control of the translation stage along the y and z axes we can place the PET in a region of space where the particle is right at the central maximum of the TEM$_{00}$ Gaussian mode beam. Keeping the particle at that point the τ_λ will reach its lowest value and from there the measurement process will begin while the particle size evolves in the case of our experiment.

7

1 Figure 2 shows for the 532-CRDS system the deep depression of the τ_{532} values when the
2 particle is carefully aligned to the center of the TEM$_{00}$ mode profile of the Gaussian beam.
3 The lowest τ_{532} value in the cavity is due to several reasons: to the characteristic value of
4 $\tau_{0,532}$ for the cavity, to the τ_{532} dependence on the laser wavelength since the attenuation
5 of the signal will depend on key parameters of the particle such as size and n_{532}, the latter
6 depending on the wavelength. The larger τ_{532} values like $\tau_{0,532}$ values denote that the
7 particle is completely outside the central maximum of the TEM$_{00}$ Gaussian mode beam.
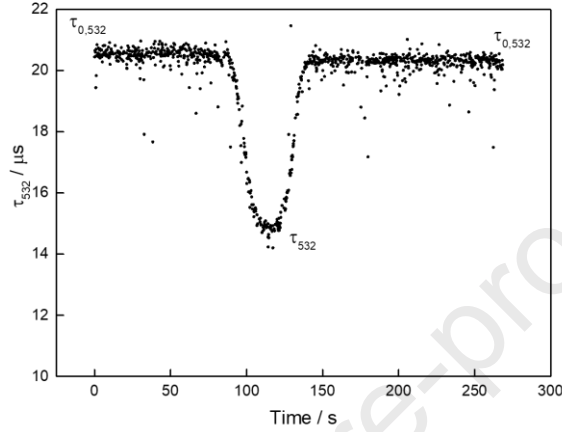
8

9

10

11

12

13

14

15

16

17 **Figure 2**. Example of τ_{532} measured for one 1,2,6-hexanetriol particle when it is outside the TEM$_{00}$
18 Gaussian beam and when it interacts with the center of the Gaussian mode peak.

19

20 **3.2. Dynamic change of the σ_{ext}.**

21 In a first step, we measured the τ_{λ} of a single levitated HT particle at 532-CRDS system
22 and simultaneously collected the evolved elastic scattering at 473 nm over a time scale of
23 ~14000 s. N_2 was continuously flowing throughout the measurement period to ensure
24 that there was no water content in the particle and the evaporated HT did not accumulate
25 in the chamber. The $\sigma_{ext,532}$ of the particle is calculated using Eq. (1). Figure 3a shows
26 the evolving HT radius over time during the evaporation process. The radius r of the
27 trapped particle is obtained from the best fit to the experimental PF from a simulated
28 library of PFs obtained from Mie theory across a realistic range of r and n_{473}. Maximizing
29 the Pearson correlation coefficient by searching a grid of n_{473} and r values will provide
30 with the best-fit n_{473} and r values for each PF. More details about the fitting procedure
31 can be found in (Valenzuela et al., 2020).

32 Figure 3b shows the scatter graph of the τ_{532} over time. The first change we observed
33 was a moderate increase in τ_{532} which is explained by the fact that during the evaporation
34 process the particle reduced its size. In addition to this decrease in τ_{532}, it was
35 accompanied by fluctuations with different resonance peaks related to that particle
36 evaporated to specific sizes for which it behaved as an optical cavity resonant with the
37 CRDS laser. The evolution of the τ_{532} measurements have a certain width due to the
38 Brownian motion of the particle passing through different phases of the standing wave,
39 which correspond to the boundaries of the particle envelope centered at a node or at an

8

antinode and points in between. After finishing the measurement, the particle was carefully separated from the center of the TEM$_{00}$ Gaussian mode and the $\tau_{0,532}$ was measured subsequently for 3 minutes.

Figure 3c shows measured $\sigma_{ext,532}$ sets (red dots) and the best-fit $\sigma_{ext,532,Mie}$ (green line) envelopes according to the procedure described in Sect. 2. Overall, the trend of $\sigma_{ext,532}$ was explained by the shrinking in size of the particle. During evaporation process, $\sigma_{ext,532}$ was expected to decrease because the geometric cross section of particle became smaller. The extinction capacity decreased on average from $2.1 \cdot 10^{-11}$ m^2 to $0.8 \cdot 10^{-11}$ m^2 when particle size decreased its radius from ~1797 nm to ~936 nm. We take advantage of the occurrence of resonant peaks for comparing with Mie theory, thus finding a value $n_{532} = 1.489$.
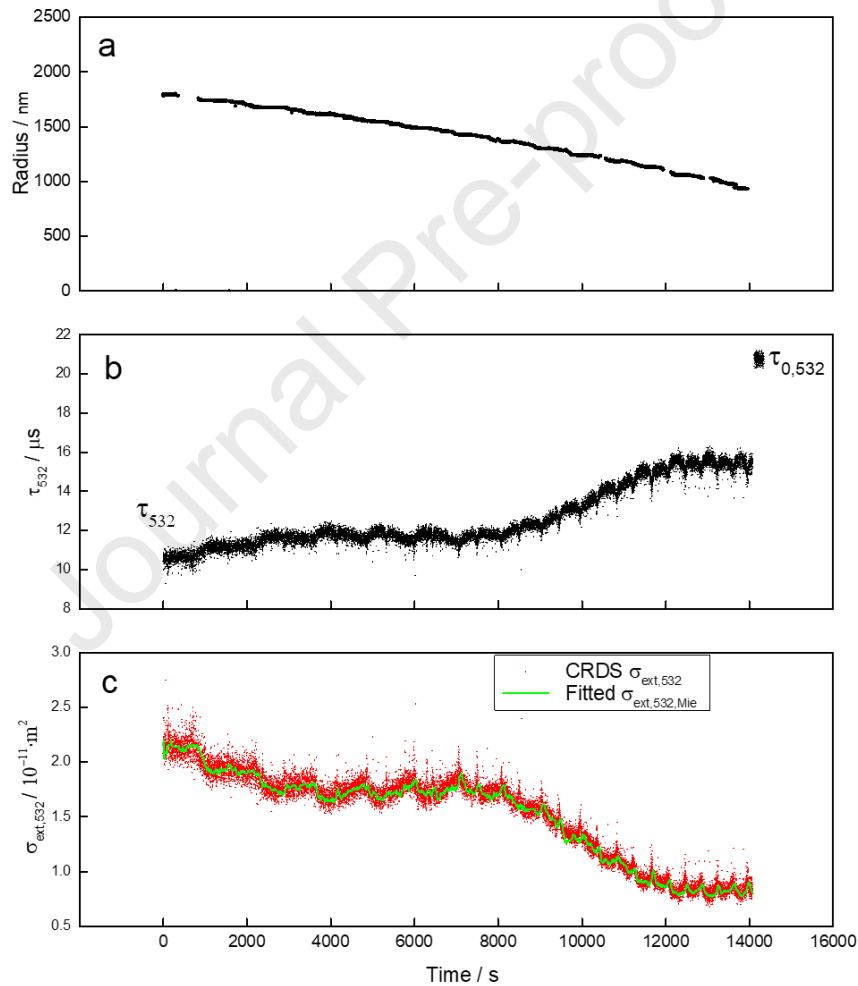
Figure 3. a) The fitted radius, b) τ_{532} and c) the comparison between the $\sigma_{ext,532,1Hz}$ and fitted $\sigma_{ext,532,Mie}$ versus time for one 1,2,6-hexanetriol particle.

9

3.3. Wavelength dependence of σ_{ext}.

A HT particle was trapped and optically aligned with the 532 nm-CRDS system. The experiment lasted about 4000 s during which the HT particle evaporated under RHs < 10% and elastic scattering (phase function) at 473 nm and the $\sigma_{ext,532}$ were measured simultaneously.

Figures 4 a, b, c and d show the artistic scheme of procedure, the fitted *r*, the τ_{532} measurements and $\sigma_{ext,532}$ data (green dots) being the red line the fitted $\sigma_{ext,532,Mie}$, respectively, for the HT particle over time. According to the 473 nm phase function fit, particle was trapped with an initial radius of 1850 nm with a value retrieved for n_{473} of 1.478. This size caused a depression in τ_{532} parameter up to values of ~ 12 µs. That was translated to values of $\sigma_{ext,532}$ slightly above of $1.5 \cdot 10^{-11}$ m^2. The comparison of $\sigma_{ext,532,1Hz}$ with $\sigma_{ext,532,Mie}$ provided a value of n_{532} of 1.476. HT evaporated over time which is indicated by the decreasing trend in *r* and the slightly increasing one in τ_{532}. Immediately afterwards, keeping the same particle trapped, the PET was moved to the 405 nm-CRDS system. Again, the PET and particle were optically aligned with the ultraviolet CRDS system. This process took approximately 20 minutes before proceeding to the next set of measurements. Elastic scattering at 532 nm and $\sigma_{ext,405}$ were collected during approximately 2800 s. Figures 4 e, f, g and h show the artistic scheme of the procedure, the fitted *r*, the τ_{405} measurements and $\sigma_{ext,405}$ data (purple dots) being the black line the fitted $\sigma_{ext,405,Mie}$, respectively, for the HT particle over time. The fitting of phase function with Mie theory provided a value $n_{532} = 1.481$ whereas the comparison of $\sigma_{ext,405,1Hz}$ with $\sigma_{ext,405,Mie}$ provided a value $n_{405} = 1.489$. Although some time elapsed between the two experiments due to the time needed to correctly align the optical system and even though the particle continued to evaporate, we can perfectly appreciate the continuity in the trend of the fitted radius and $\sigma_{ext,\lambda}$ in the two data sets, which provides confidence in our results. This experiment demonstrated the stability, reproducibility, and robustness of the combined PET and D-CRDS setup, which allowed to retrieve rigorous optical information and dynamic changes in $\sigma_{ext,\lambda}$ of the same particle over time and its spectral dependence.
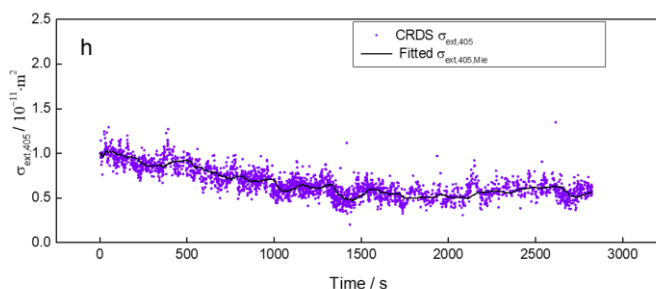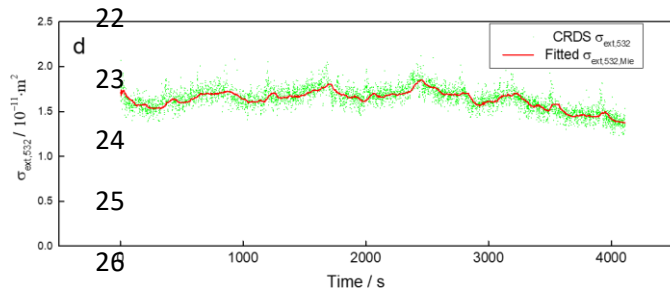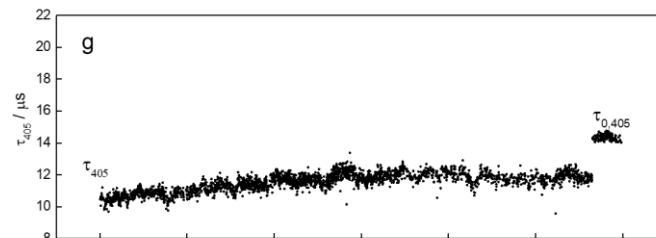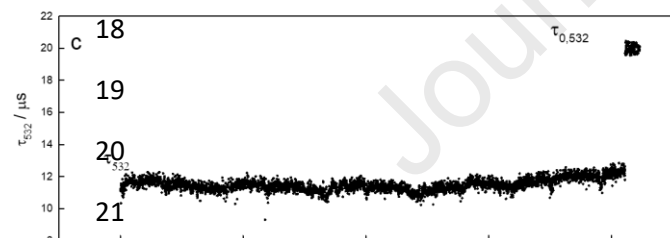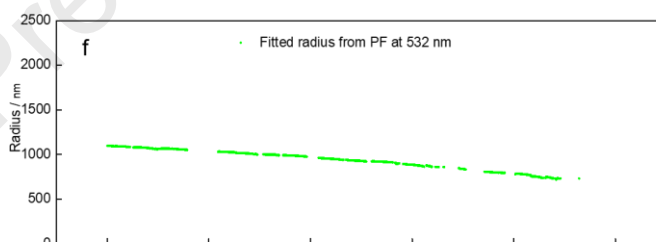
1

2

3

4
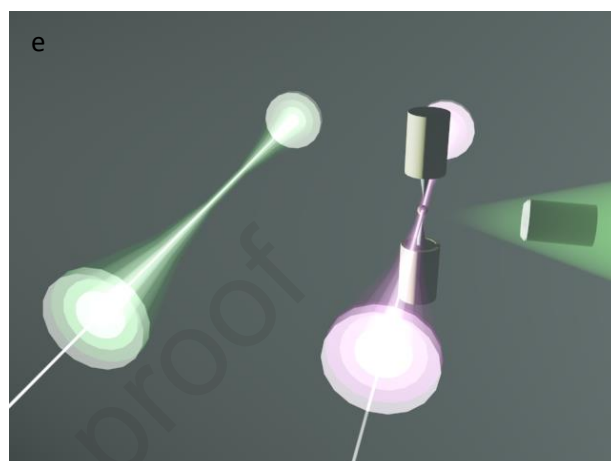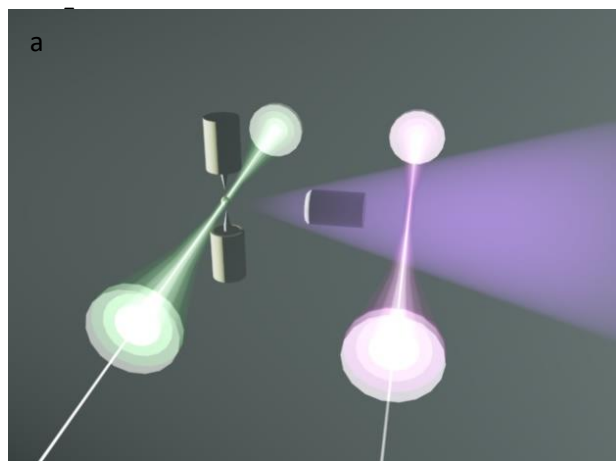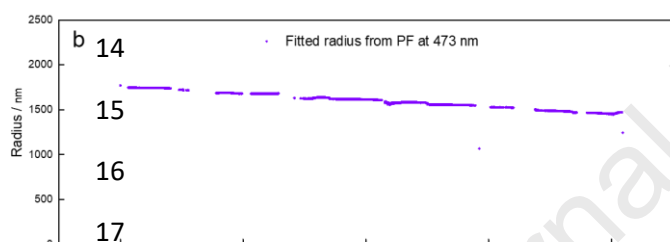
Figure 4. a-d) Artistic representation of measurements in the 532-CRDS system, fitted radius, τ_{532}, and the comparison between the $\sigma_{ext,532,1Hz}$ and fitted $\sigma_{ext,532,Mie}$ versus time. e-h) Artistic representation of measurements in the 405-CRDS system, fitted radius, τ_{405} and comparison between $\sigma_{ext,405,1Hz}$ and the fitted $\sigma_{ext,405,Mie}$ versus time, for one 1,2,6-hexanetriol particle.

32

11

3.4. Hygroscopic behavior of a sodium chloride particle

Figure 5 investigates the transformation of a levitated sodium chloride particle as it is exposed to dehydration and hydration processes into air. To this aim, we measured the changes in τ_{532} upon varying RH in a controlled manner by controlling the ratio between dry and wet N_2 fluxes. To gain additional information about changes in size and refractive index, we continuously monitored the elastic scattering at 473 nm during the whole experiment (Figure 5).

The particle is initially captured at an RH of 75.8% and the change in τ_{532} was registered by the 532-CRDS system over a time scale of ~8700 s as the RH was allowed to perform one full hygroscopic cycle (dehydration and hydration). The particle radius and n_{473} was determined from analysis of the PFs. The initial particle radius was determined to be ~ 1510 nm with a value for n_{473} =1.3661, close to that of pure water (region I Figure 5a). At high RHs the weight of solute is low relative to the total aqueous particle. Regarding CRDS measurements, the first change that we observed was a moderate increase of τ_{532} with fluctuations when the RH was reduced. As we can see in figure 5b (Region I), the τ_{532} showed the typical structure of a standing wave with the particle crossing several nodes and antinodes and the region between them. From Eq. 1 we calculated the $\sigma_{ext,532}$ for the complete experiment. In this case the trend of the $\sigma_{ext,532}$ depends not only on the evolution of the size of the aqueous sodium chloride particle but also on the change of the n_{532}. As the particle evaporates, the solute weight concentration becomes more important and therefore there was a dependence of n_{532} on the RH. During the dehydration process, the sodium chloride particle lost water and reduced its size. This resulted in an increase in $\tau_{532,dehydration}$ values until a state is reached where the particle stops losing water (see at the end of region I around t = 2683 s in Figure 5). If the RH was further reduced below 51.6%, the $\tau_{532,dehydration}$ underwent a rapid and reversible change. The particle mass and charge of the particle dropped rapidly, as observed in other setups upon changing conditions (Ricci et al., 2019). In parallel, we independently observed a sudden scatter in particle radius estimation and n_{473} (region II Figure 5a). In this RH the particle is mostly dry and is no longer a sphere and Mie theory was not valid to fit experimental phase function data. This point is known as efflorescence (region II in figure 5) and thereafter the $\tau_{532,efflorescence}$ values remained stable and independent of reductions of the surrounding RH. Nevertheless, from $\tau_{532,efflorescence}$ was posible to calculate $\sigma_{ext,efflorescence}$. Although we have measurements from a single particle of irregular geometry, a limitation arises because the scattering cross section depends on the orientation of the particle with respect to the incident laser beam. Due to Brownian motion, the orientation of an irregular particle stored in the Paul trap changes randomly over time, and the measured scattering will be an average over all possible orientations of the particle (Birdsall et al., 2018). Linking to the natural atmosphere, aerosol particles are generally regarded as randomly oriented in the space, so the scattering parameters of the atmospheric particles in the radiative transfer models should be averaged over different orientations to obtain the representative values. In this line, a non-spherical code as T-Matrix has incomparable advantage because it is a method that not only is independent of particle's orientation and incident light, but also contains all the scattering information of non-spherical particles (Hu et al., 2020; Mishchenko and Travis, 1998).

1 Therefore, experimental extinction and scattering cross section measurements retrieved
2 from particle levitated in Paul trap can be directly fitted to theoretical data modeled with
3 T-Matrix code. We incorporated the comparison of $\sigma_{ext,532,1Hz}$ with
4 $\sigma_{ext,532,Mie}$ (green line) for the complete experiment even in eflorescence region.
5 However, a non-spherical T-Matrix code would be recommendable to retrieve realistic
6 optical information of irregular particle. This is not the objective of this analysis and will
7 be the subject of a future work. Again, RH was increased and just when it raised to ~
8 70.6% non-spherical sodium chloride particle began to take up water and increase in size.
9 Mie theory worked once again and r and n_{473} were fitted from experimental phase
10 functions (region III in figure 5a). RH raised a final value of 89.6 % and τ_{532} reached
11 lower values than the initital experiment. Finally, the particle was ejected and $\tau_{0,532}$
12 reaches typical empty cavity values.
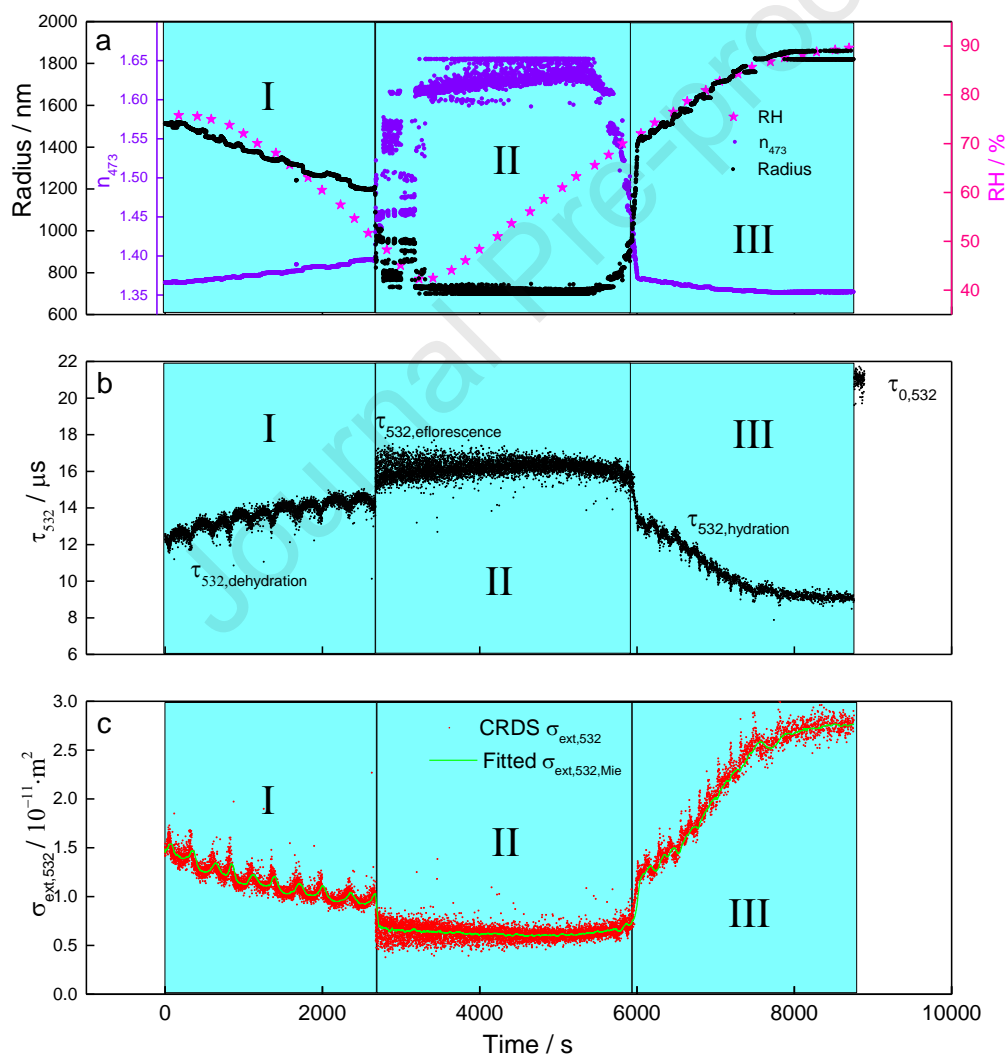
13

14 **Figure 5**. a) Fitted radius, b) τ_{532} and c) the comparison between the $\sigma_{ext,532,1Hz}$ and fitted $\sigma_{ext,532,Mie}$
15 versus time for one sodium chloride particle.

16

13

4. CONCLUSIONS

We present a new setup combining a Paul electrodynamic trap (PET) and a double-cavity D-CRDS for the spectroscopic observation of single particles suspended in air and optically interrogated for an indefinite time. With this new setup we addressed three open questions on the optical properties of aerosol particles. First, we obtained refined measurements of the size and $\sigma_{ext,532}$ of individual particles levitated by HT from simultaneous elastic scattering and τ_{532}. Second, we were able to obtain measurements of elastic scattering and extinction cross sections in each of the cavities while keeping the same trapped particle. The PET can move on a rail transverse to the two parallel cavities with the initially trapped particle held stationary and levitating in the trap. The robustness of the PET made it easy to manipulate and control the particle with high sensitivity, keeping the particle only interacting with the central maximum of two TEM$_{00}$ Gaussian modes independent of the cavities. Although some time elapsed between the two experiments due to the need for proper optical alignment of the setup and even though the particle continued to evaporate, we can perfectly appreciate the continuity in the trend of the fitted radius and $\sigma_{ext,\lambda}$ in the two data sets, which provides confidence in our system. This experiment demonstrated the stability, reproducibility, and robustness of the combined PET and D-CRDS setup which allowed to retrieve rigorous optical information and dynamic change of $\sigma_{ext,\lambda}$ of the same particle over time and its spectral dependence. Third, we gained knowledge about scale time of the changes affecting mass, density, refractive index about a sodium chloride particle during dehydration and hydration cycles from elastic scattering and $\tau_{532,dehydration}$. Further, we obtained crucial information of $\sigma_{ext,532}$ when particle became irregular in morphology which is demonstrated on this study.

AUTHOR INFORMATION

Corresponding Author

[+,‡,*]**Antonio Valenzuela**- *Andalusian Institute for Earth System Research (IISTA-CEAMA) and Department of Applied Physics, University of Granada, Granada, 18071, Spain;* orcid.org/0000-0003-0290-4081; Email: avalenzuela@ugr.es

Author Contributions

The manuscript was written through contributions of all authors. All authors have given approval to the final version of the manuscript. [+,‡]These authors contributed equally.

1   [+,‡]**Elena Bazo**- *Andalusian Institute for Earth System Research (IISTA-CEAMA) and*

2   *Department of Applied Physics, University of Granada, Granada, 18071, Spain;*

3   orcid.org/0000-0003-1831-6874; Email: ebazo@ugr.es

4   [‡]**Raul A. Rica**- *Universidad de Granada, Department of Applied Physics and research*

5   *unit Modelling Nature (MNat) , Granada, 18071, Spain;* orcid.org/0000-0003-1831-

6   6874; Email: rul@ugr.es

7   [+,‡]**Lucas Alados-Arboledas**- *Andalusian Institute for Earth System Research (IISTA-*

8   *CEAMA) and Department of Applied Physics, University of Granada, Granada, 18071,*

9   *Spain;* orcid.org/ 0000-0003-3576-7167; Email: alados@ugr.es

10   [+,‡]**Francisco José Olmo-Reyes-** *Andalusian Institute for Earth System Research (IISTA-*

11   *CEAMA) and Department of Applied Physics, University of Granada, Granada, 18071,*

12   *Spain;* orcid.org/ 0000-0002-0186-1721; Email: fjolmo@ugr.es

13   **Notes**

14   The authors declare no competing financial interest.

15   **ACKNOWLEDGMENTS**

25   **REFERENCES**

26

27   Archer, J., Walker, J.S., Gregson, F.K.A., Hardy, D.A., Reid, J.P., 2020. Drying kinetics
28   and particle formation from dilute colloidal suspensions in aerosol droplets.
29   Langmuir 36, 12481–12493. https://doi.org/10.1021/acs.langmuir.0c01830

1 Bain, A., Rafferty, A., Preston, T.C., 2018. Determining the size and refractive index of
2   single aerosol particles using angular light scattering and Mie resonances. J Quant
3   Spectrosc Radiat Transf 221, 61–70. https://doi.org/10.1016/j.jqsrt.2018.09.026

4 Bykov, D., Dania, L., Mestres, P., Northup, T., 2019. Laser cooling of secular motion of
5   a nanoparticle levitated in a Paul trap for ion-assisted optomechanics. Proceedings
6   of SPIE - The International Society for Optical Engineering 11083.
7   https://doi.org/10.1117/12.2528141

8 Cachorro, V.E., Vergaz, R., De Frutos, A.M., 2001. A quantitative comparison of a-(A
9   A turbidity parameter retrieved in different spectral ranges based on
10   spectroradiometer solar radiation measurements, Atmospheric Environment.

11 Conangla, G.P., Alarcón, R.A., Quidant, R., 2020. Extending vacuum trapping to
12   absorbing objects with hybrid Paul-optical traps. arXiv preprint arXiv:2005.05486.

13 Conangla, G.P., Schell, A.W., Rica, R.A., Quidant, R., 2018. Motion control and optical
14   interrogation of a levitating single nitrogen vacancy in vacuum. Nano Lett 18,
15   3956–3961.

16 Cotterell, M.I., Knight, J.W., Reid, J.P., Orr-Ewing, A.J., 2022. Accurate Measurement
17   of the Optical Properties of Single Aerosol Particles Using Cavity Ring-Down
18   Spectroscopy. Journal of Physical Chemistry A 126, 2619–2631.
19   https://doi.org/10.1021/acs.jpca.2c01246

20 Cotterell, M.I., Szpek, K., Haywood, J.M., Langridge, J.M., 2020. Sensitivity and
21   accuracy of refractive index retrievals from measured extinction and absorption
22   cross sections for mobility-selected internally mixed light absorbing aerosols.
23   Aerosol Science and Technology 54, 1034–1057.
24   https://doi.org/10.1080/02786826.2020.1757034

25 Cotterell, M.I., Willoughby, R.E., Bzdek, B.R., Orr-Ewing, A.J., Reid, J.P., 2017. A
26   complete parameterisation of the relative humidity and wavelength dependence of
27   the refractive index of hygroscopic inorganic aerosol particles. Atmos Chem Phys
28   17, 9837–9851. https://doi.org/10.5194/acp-17-9837-2017

29 David, G., Esat, K., Ritsch, I., Signorell, R., 2016. Ultraviolet broadband light scattering
30   for optically-trapped submicron-sized aerosol particles. Physical Chemistry
31   Chemical Physics 18, 5477–5485. https://doi.org/10.1039/c5cp06940h

32 Davies, J.F., 2019. Mass, charge, and radius of droplets in a linear quadrupole
33   electrodynamic balance. Aerosol Science and Technology 53, 309–320.
34   https://doi.org/10.1080/02786826.2018.1559921

35 Dinar, E., Riziq, A.A., Spindler, C., Erlick, C., Kiss, G., Rudich, Y., 2008. The complex
36   refractive index of atmospheric and model humic-like substances (HULIS)
37   retrieved by a cavity ring down aerosol spectrometer (CRD-AS). Faraday Discuss
38   137, 279–295.

39 Gong, Z., Pan, Y. Le, Videen, G., Wang, C., 2018. Optical trapping and manipulation of
40   single particles in air: Principles, technical details, and applications. J Quant
41   Spectrosc Radiat Transf. https://doi.org/10.1016/j.jqsrt.2018.04.027

16

1 Gong, Z., Pan, Y.-L., Wang, C., 2017. Characterization of single airborne particle
2   extinction using the tunable optical trap-cavity ringdown spectroscopy (OT-CRDS)
3   in the UV. Opt Express 25, 6732. https://doi.org/10.1364/oe.25.006732

4 Gregson, F.K.A., Robinson, J.F., Miles, R.E.H., Royall, C.P., Reid, J.P., 2018. Drying
5   Kinetics of Salt Solution Droplets: Water Evaporation Rates and Crystallization. J
6   Phys Chem B 123, 266–276.

7 Hart, M.B., Sivaprakasam, V., Eversole, J.D., Johnson, L.J., Czege, J., 2015. Optical
8   measurements from single levitated particles using a linear electrodynamic
9   quadrupole trap. Appl Opt 54, F174–F181.

10 Hasenkopf, C.A., Beaver, M.R., Trainer, M.G., Langley Dewitt, H., Freedman, M.A.,
11   Toon, O.B., McKay, C.P., Tolbert, M.A., 2010. Optical properties of Titan and
12   early Earth haze laboratory analogs in the mid-visible. Icarus 207, 903–913.
13   https://doi.org/10.1016/j.icarus.2009.12.015

14 Hu, S., Liu, L., Gao, T., Zeng, Q., Liu, X., 2020. An efficient implementation of the
15   light scattering simulation for random-oriented non-rotationally symmetric
16   particles using invariant imbedding T-matrix method. J Quant Spectrosc Radiat
17   Transf 241. https://doi.org/10.1016/j.jqsrt.2019.106734

18 Knight, J.W., Egan, J. V., Orr-Ewing, A.J., Cotterell, M.I., 2022. Direct Spectroscopic
19   Quantification of the Absorption and Scattering Properties for Single Aerosol
20   Particles. Journal of Physical Chemistry A 126, 1571–1577.
21   https://doi.org/10.1021/acs.jpca.2c00532

22 Krieger, U.K., Braun, C., 2001. Light-scattering intensity fluctuations in single aerosol
23   particles during deliquescence. J Quant Spectrosc Radiat Transf 70, 545–554.
24   https://doi.org/10.1016/S0022-4073(01)00028-0

25 L. Price, C., Bain, A., J. Wallace, B., C. Preston, T., F. Davies, J., 2020. Simultaneous
26   Retrieval of the Size and Refractive Index of Suspended Droplets in a Linear
27   Quadrupole Electrodynamic Balance. J Phys Chem A 124, 1811–1820.
28   https://doi.org/10.1021/acs.jpca.9b10748

29 Lin, J., Hart, A.G., Li, Y.Q., 2015. Optical pulling of airborne absorbing particles and
30   smut spores over a meter-scale distance with negative photophoretic force. Appl
31   Phys Lett 106. https://doi.org/10.1063/1.4919533

32 Mason, B.J., Cotterell, M.I., Preston, T.C., Orr-Ewing, A.J., Reid, J.P., 2015. Direct
33   measurements of the optical cross sections and refractive indices of individual
34   volatile and hygroscopic aerosol particles. J Phys Chem A 119, 5701–5713.

35 Mason, B.J., King, S.-J., Miles, R.E.H., Manfred, K.M., Rickards, A.M.J., Kim, J.,
36   Reid, J.P., Orr-Ewing, A.J., 2012. Comparison of the accuracy of aerosol refractive
37   index measurements from single particle and ensemble techniques. J Phys Chem A
38   116, 8547–8556.

39 Miles, R.E.H., Carruthers, A.E., Reid, J.P., 2011. Novel optical techniques for
40   measurements of light extinction, scattering and absorption by single aerosol
41   particles. Laser Photon Rev 5, 534–552.

17

1 Millen, J., Monteiro, T., Pettit, R., Vamivakas, A., 2020. Optomechanics with levitated
2   particles. Reports on Progress in Physics 83. https://doi.org/10.1088/1361-
3   6633/ab6100

4 Mishchenko-, M.I., Travis, L.D., 1998. CAPABILITIES AND LIMITATIONS OF A
5   CURRENT FORTRAN IMPLEMENTATION OF THE [1]-MATRIX METHOD
6   FOR RANDOMLY ORIENTED, ROTATIONALLY SYMMETRIC
7   SCATTERERS, J. Quant. Spectrosc. Radiat. [1]ransfer.

8 Pettersson, A., Lovejoy, E.R., Brock, C.A., Brown, S.S., Ravishankara, A.R., 2004.
9   Measurement of aerosol optical extinction at 532nm with pulsed cavity ring down
10   spectroscopy. J Aerosol Sci 35, 995–1011.

11 Ricci, F., T. Cuairan, M., P. Conangla, G., W. Schell, A., Quidant, R., 2019. Accurate
12   Mass Measurement of a Levitated Nanomechanical Resonator for Precision Force-
13   Sensing. Nano Lett 19, 6711–6715. https://doi.org/10.1021/acs.nanolett.9b00082

14 Schuster, G.L., Dubovik, O., Holben, B.N., 2006. Angstrom exponent and bimodal
15   aerosol size distributions. Journal of Geophysical Research Atmospheres 111.
16   https://doi.org/10.1029/2005JD006328

17 Valenzuela, A., Chu, F., Haddrell, A., Cotterell, M., Walker, J., Orr-Ewing, A., Reid, J.,
18   n.d. Optical Interrogation of Single Levitated Droplets in a Linear Quadrupole
19   Trap by Cavity Ring-Down Spectroscopy. J Phys Chem A 125, 394–405.
20   https://doi.org/10.1021/acs.jpca.0c09213

21 Valenzuela, A., Olmo, F.J., Lyamani, H., Antón, M., Titos, G., Cazorla, A., Alados-
22   Arboledas, L., 2015. Aerosol scattering and absorption Angström exponents as
23   indicators of dust and dust-free days over Granada (Spain). Atmos Res 154.
24   https://doi.org/10.1016/j.atmosres.2014.10.015

25 Valenzuela, A., Rica, R.A., Olmo-Reyes, F.J., Alados-Arboledas, L., 2020. Testing a
26   Paul trap through determining the evaporation rate of levitated single semi-volatile
27   organic droplets. Opt Express 28, 34812. https://doi.org/10.1364/OE.410590

28 Walker, J.S., Carruthers, A.E., Orr-Ewing, A.J., Reid, J.P., 2013. Measurements of light
29   extinction by single aerosol particles. J Phys Chem Lett 4, 1748–1752.

30 Zardini, A.A., Krieger, U.K., Marcolli, C., 2006. White light Mie resonance
31   spectroscopy used to measure very low vapor pressures of substances in aqueous
32   solution aerosol particles. Opt Express 14, 6951.
33   https://doi.org/10.1364/oe.14.006951

34

35

36

Double Cavity ring down time data were measured for the same single aerosol particle for the first time.

The dependency on relative humidity was calculated for extinction cross sections.

Refractive index was retrieved from the fit with Mie theory

The authors declare that they have no known competing financial interests or personal relationships that could have appeared to influence the work reported in this paper.